View Article Online
View Journal

# Nanoscale Horizons

The home for rapid reports of exceptional significance in nanoscience and nanotechnology

## Accepted Manuscript

This article can be cited before page numbers have been issued, to do this please use: N. Osterloh, M. Vyshnepolsky, T. Pan and K. Morgenstern, *Nanoscale Horiz.*, 2026, DOI: 10.1039/D5NH00836K.

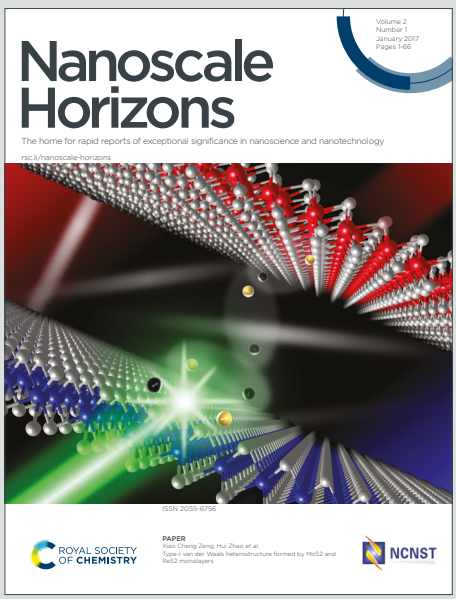

New Concepts Statement

View Article Online
DOI: 10.1039/D5NH00836K

The use of high-intensity ultra-fast lasers for material processing is well-established and has even been adopted in industrial applications. However, research continues into how the interaction between light and material leads to changes at the nanoscale. By examining an irradiated surface with the high spatial resolution of a scanning tunneling microscope at low temperatures below 10 K, where thermal motion is minimized, we can observe nanoscale clusters formed from material ejected from the bulk to the surface through a non-thermal process. The quantity of these clusters is influenced by the local nanoscale fluence. Interestingly, we identify a broad range of fluence, where the amount of material ejected from the bulk does not depend on fluence levels. This fluence-independent range is crucial for manipulating matter at the nanoscale using ultra-short laser pulses. We propose utilizing low-intensity femtosecond laser illumination to design tailored nanoclusters.



View Article Online
DOI: 10.1039/D5NH00836K

Journal Name

ARTICLE TYPE

Cite this: DOI: 00.0000/xxxxxxxxxx

# Fluence-independent range of surface roughening within the Gaussian-shaped profile of a low-intensity ultrashort laser

N. Osterloh, M. Vyshnepolsky, T. Pan,‡ and K. Morgenstern*

Received Date
Accepted Date

DOI: 00.0000/xxxxxxxxxx

In the pursuit to master the manipulation of matter at the nanoscale, we investigate the local effects of irradiating a Cu(511) surface with a Gaussian-shaped laser spot lasting 50 fs at a fluence well beneath the ablation threshold. Irradiation results in the formation of adatom and vacancy clusters. Such changes exhibit significant variation based on their position within the laser spot because of a strong dependence on the locally absorbed fluence, limiting the precision of nanoscale modifications induced by laser irradiation. We delve into these critical nanoscale transformations across the microscale using the nanoscale resolution of low-temperature scanning tunneling microscopy. We identify a broad fluence range, where the number of defects stays approximately constant. Our results open a route to create defined nanostructures across a larger spatial range despite the inevitable fluence variations across a Gaussian-shaped laser spot.

## 1 Introduction

The interaction of short pulse lasers with metals is important both scientifically and practically[1]. Practical applications include the creation of unique surface morphologies through processes such as nanoablation and photolithography[2,3]. From a scientific perspective, studying how materials respond to femtosecond (fs) laser irradiation offers invaluable insights into material behavior under extreme conditions of ultrahigh peak power and ultrashort pulse duration. Under these conditions, ultrashort laser irradiation drives materials into new states of matter far from equilibrium[4], leading to structural changes that cannot occur under equilibrium conditions[5–7]. These structural modifications create unique properties through the surfaces formed on the irradiated materials[8–10]. Gaining insight into the processes leading to structural changes is crucial for uncovering the non-equilibrium properties of various materials[11,12]. Consequently, this research sits at the forefront of condensed matter physics and nanoscale materials science[13].

The explored effects resulting from the interaction of fs laser light with matter are fs laser-induced ion emission[14], photodynamic assembly[15], in situ anisotropic laser printing[16], and the optical response of nanostructures[17], amongst others. Moreover, the interaction of surfaces with their environment significantly influences the material's behavior in various applications, including catalysis[6], friction[10,18,19], and coatings[20]. The various phenomena and their applications will profit from a homogeneous surface modification across the region of interest.

The energy densities used to modify the surface structure using fs laser pulses typically exceed the thresholds for melting and ablation. For copper (Cu), the material examined in this study, the ablation threshold is approximately 1.7 J/cm$^2$ at a wavelength of 800 nm[21]. At these high laser fluences, surface damage occurs through heat-induced stress confinement, where the heating time is shorter than the time needed for mechanical equilibration of the heated area. This thermal process is primarily influenced by the energy transfer between the excited electrons and the cooler lattice[3,21].

Ultrafast melting of various materials at these high laser powers far exceeding that we are employing here has been extensively studied to uncover the fundamental microscopic mechanisms involved[22]. Researchers have utilized scanning and transmission electron microscopy (SEM and TEM) to image the microstructures on surfaces following laser melting[23]. These observations provided valuable data for simulations using atomistic molecular dynamics, which aim to achieve an atomic-level understanding of the melting process[24,25]. Significantly underexplored are the microscopic details of the recently unraveled phenomenon on changes to the surface texture at absorbed fluences far below the ablation threshold[26].

In our recent investigation of fs laser-induced changes on a Ag(100) surface far below the ablation threshold, we utilized scanning tunneling microscopy (STM) to reveal nanoscale sur-

Ruhr-Universität Bochum, Physikalische Chemie I, D-44780 Bochum, Germany. Tel: +49-2343225529; E-mail: karina.morgenstern@rub.de
‡ present address: Shenzhen Institute for Quantum Science and Engineering and Department of Physics, Southern University of Science and Technology, Shenzhen 518055, China.

View Article Online
DOI: 10.1039/D5NH00836K



face modifications[27]. The process underlying the surface modifications begins with the creation of vacancies and interstitials in the bulk material, which are subsequently driven to the surface in response to subsequent laser pulses. The surface adatoms formed were further driven to diffuse and agglomerate. Finally, also the agglomerates were driven to diffuse across the surface. A dependence on the locally absorbed fluence resulted in differing island shapes on the Cu(111) surface in different regions of the laser spot[28]. Such local changes oppose the quest to create defined nanostructures across a surface range.

In this article, we investigate the structures induced by fs laser pulses on the vicinal Cu(511) surface across a laser spot to characterize the fluence-dependent behavior of the bulk-created vacancies and interstitials driven to the surface. Our findings reveal that the yield of laser-induced surface defects exhibits a complex non-linear and non-monotonous relationship with fluence. We identify a fluence range where the amount of material driven to the surface hardly depends on absorbed fluence, a range of potential use in various applications.

## 2 Experimental Methods

STM measurements are performed under ultrahigh vacuum (UHV) with a base pressure of less than $2 \cdot 10^{-10}$ mbar, utilizing a low-temperature beetle-type STM that allows direct optical access to the sample[29], a system developed to alter and analyze matter at the nanoscale[30].

The Cu(511) surface is cleaned by repeated cycles of $Ne^+$ sputtering and annealing. Sputtering is performed for 45 min at a partial neon pressure of $3 \cdot 10^{-5}$ mbar, with an acceleration voltage set to 1 keV and a sputtering current of 3 $\mu$A. After sputtering, the sample is flashed to 850 K and annealed for a few minutes at 720 K. Following this preparation, the sample is cooled to approximately 50 K and transferred into the STM, where measurements are performed at 7 K.

The commercial laser, REGA 9050 from Coherent, emits laser pulses at a wavelength of 800 nm with a repetition rate of 250 kHz. It has a maximum power output of 1.5 W, delivering a pulse energy of 6 $\mu$J. The frequency-doubled laser light (400 nm) is focused below the tip by mirrors close to the tip within the cryostat shields. The pulse width at 400 nm is approximately 50 fs at the sample surface, as measured in an in-situ auto-correlation experiment.

The typical cooling times for phonon systems on metal surfaces at cryogenic temperatures, given our laser parameters, are of the order of 10 ps[31]. This means that the system reaches full equilibrium long before the next laser pulse strikes the surface, allowing each pulse to be treated as a separate experiment. This scenario contrasts significantly with laser-excitation experiments conducted at higher fluence and temperature on silicon surfaces, where the final surface morphology is influenced by the repetition rate[32].

The sample is irradiated for 1 s to 4 s with the tip retracted as far away as possible from both the scanned area and the incoming laser light. The absorbed fluences are 7.8 mJ/cm$^2$ or 9 mJ/cm$^2$, taking into account the 72% absorption of copper at 400 nm using p-polarized light at a 65° incident angle. These absorbed fluences correspond to the average fluences conventionally reported within the $1/e^2$ diameter of the laser spot The locally absorbed fluence varies across the Gaussian-shaped laser spot, reaching double the average value at its peak. Due to the 65° incident angle, the laser spot appears elliptical on the surface, with an eccentricity of 0.82 as determined from the photoelectron signal. The main axis of the ellipsoid is oriented at 60° angles to the x axes of the STM.

After irradiation, the irradiated area is imaged using a newly developed procedure that addresses the limited range of low-temperature STMs, starting at a position, defined (0,0), with the tip positioned at (-1.215 $\mu$m,+1.215 $\mu$m) during irradiation[28]. In our beetle-type STM, the imaging range is confined to a relatively small area of 300 nm by 300 nm, within a total area of 1 $\mu$m$^2$, due to the maximum voltage of $\pm$200 V that can be applied to the scanning piezos. We extend the imaging range by employing a slip-stick motion of the plate that holds the tip to investigate regions with varying locally absorbed fluence within the laser spot, a spot that spans tens of micrometers. We subtly move the tip by just 300 nm to capture partially overlapping images in adjacent regions. Occasionally, we need to adjust the tip-sample distance due to a slight misalignment between the sample plane and the imaging plane, and a limited vertical dynamic range of the scanning piezo of 200 nm. This adjustment is made possible by three ramps on the plate, inclined at an angle of 2° to the plate, allowing us to approach or retract the tip by up to 0.75 mm through rotational motion.

The piezo tripod that supports the plate facilitates the slip-stick motion in an area with a diameter of 6 mm. In principle, we could image the entire surface of several mm$^2$ using this method. However, capturing a single line of images across a laser spot approximately 10 $\mu$m in length requires days to weeks of continuous measurements. This process demands not only exceptional tip stability but also that all other experimental parameters remain stable over extended periods.

Coverages are expressed in monolayers (ML), indicating the presence of one adatom per surface atom in the adsorbate layer.

## 3 Results and discussion

### 3.1 Pristine surface prior to laser irradiation

Typically, surface science studies employ low-indexed sample surfaces for their simplicity in both preparation and analysis. However, our previous work revealed that for these surfaces, laser-induced surface processes are active at the absorbed fluences necessary to induce bulk processes. We chose the vicinal Cu(511) surface here to overcome this limitation.

The Cu(511) surface is a vicinal surface to (100) planes, featuring terraces that are 0.663 nm wide, which is slightly less than three atomic distances, with $a_{Cu100}$ = 0.255 nm the atomic distance in the (100) plane (Fig. 1a). The step edges between the (100) terraces appear as stripes extending along the $[01\bar{1}]$ direction in large-scale STM images (Fig. 1b). A minor miscut of the crystal towards the (511) plane results in secondary step edges that separate different (511) planes, with a height difference of $(69.3 \pm 0.7)$ pm (Fig. 1c). The experimental height aligns with the

View Article Online
DOI: 10.1039/D5NH00836K

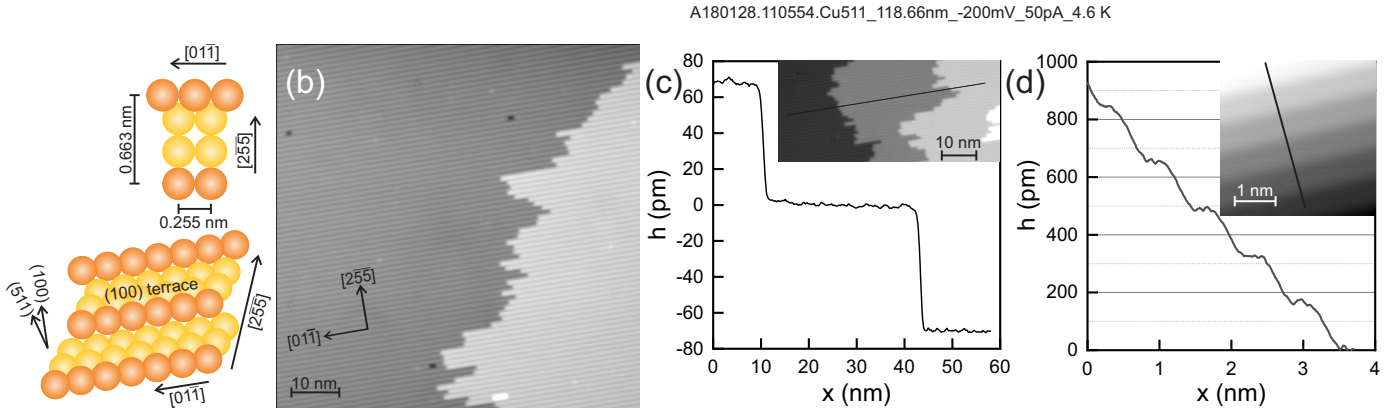


Fig. 1 Characterization of the Cu(511) surface: (a) Ball model of surface: top view (top) and 3D view in same orientation as the STM image in panel *b* (bottom); (b) STM image with one secondary step edge (c) Height profile across two secondary step edges along the line in the STM image in the inset (d) Height profile across five primary step edges along the line in the STM image in the inset; the images were recorded at (b) I = 50 pA, V = -200 mV, (c) 19 pA, 500 mV, and (d) 280 nA, -9 mV.

expected height of $1/5 \cdot a = 69$ pm. Each of the protruding fingers at the secondary step edge in Fig. 1b corresponds to one of the approximately three-atom-wide terraces. The primary step edges between the (100) terraces can only be distinguished under extreme tunneling parameters as illustrated in Fig. 1d. The average apparent height of the primary step edges of 169 pm deviates slightly from the anticipated height of the primary step edges, calculated to be 180 pm, at these tunneling parameters.

The vicinal Cu(511) surface provides a unique opportunity to effectively separate bulk processes from surface phenomena. The significant diffusion barrier present on the Cu(100) terraces, in conjunction with the elevated step density of the vicinal surface, is expected to substantially suppress the kinetic surface processes, diffusion and agglomeration, during laser irradiation on Cu(111)[28].

### 3.2 Laser-induced alteration of the surface texture

Irradiation at a fluence that is two orders of magnitude below the laser ablation threshold alters the surface texture, resulting in both protrusions and depressions (Fig. 2a). For details of coverage and fluence determination, see the supporting information. Notably, the majority of the protrusions, around 80%, are smaller than 2 nm$^2$, while only a small fraction, about 6%, exceeds 3 nm$^2$ (Fig. 2b). The area distribution of these clusters resembles the patterns observed after "nucleation and growth"[33], characterized by an asymmetric maximum and a tail extending towards larger clusters (Fig. 2b). The small size of the clusters further confirms that laser-induced surface diffusion is largely suppressed on Cu(511), unlike on Cu(111)[28].

At a similar fluence, dendritic clusters of varying heights form on the Cu(111) surface[28]. The formation of these dendrites requires the surface diffusion of individual adatoms and the diffusion of small adatom clusters. The clustering process not being activated on the Cu(511) surface, suggests that the differing thermal diffusivities of adatoms and clusters on these two surface facets are likewise relevant for laser-induced diffusion. Overall, this observation suggests that the material is deposited as individual entities onto the Cu(511) surface, from which clusters of varying sizes form without or with only limited surface diffusion[35].

We examine the same area of the surface both before and after laser irradiation to confirm that the laser-induced surface defects originate from the bulk material (Fig. 2c,d). A small number of one-terrace-wide defects created by the laser adjustment are used as markers. These defects serve as references to ensure that we image precisely the same spot on the surface before and after the laser treatment (Fig. 2c,d, circles). They are unaltered by the laser irradiation. The laser irradiation results in more substantial number of protrusions and depressions. Since the secondary edge remains largely unchanged, the additional material cannot be sourced from that area.

The height of most protrusions measures (73 ± 3) pm, which falls within the range of height differences between two (511) planes (Fig. 2e,f). This similarity suggests that the protrusions consist of copper clusters that are one plane high. Additionally, some broader protrusions exceed the height of a single plane, assigned to clusters exceeding one layer in height.

Although the depressions are imaged to a depth of (43 ± 3) pm, which is somewhat less than the height difference between planes, we argue that the holes are actually one plane deep. The smaller apparent depth is attributed to the tip convolution effect, which reduces the measured apparent depth of small structures[36]. Therefore, we categorize these depressions as vacancy clusters caused by missing atoms within the (100) terraces.

Interestingly, the area covered by adatom clusters is roughly 50% larger than that covered by vacancy clusters despite the close relationship in the formation of these two defects in the bulk as vacancy-interstitial pairs. Similar to the findings on the Ag(100) and Cu(111) surfaces examined previously, the difference in the number of visible adatom and vacancy clusters confirms a subsurface origin[27,28]. This implies that, on Cu(511) as well, the clusters arise from vacancy-interstitial pairs that are initially created below the surface and are subsequently driven to the surface by

View Article Online
DOI: 10.1039/D5NH00836K



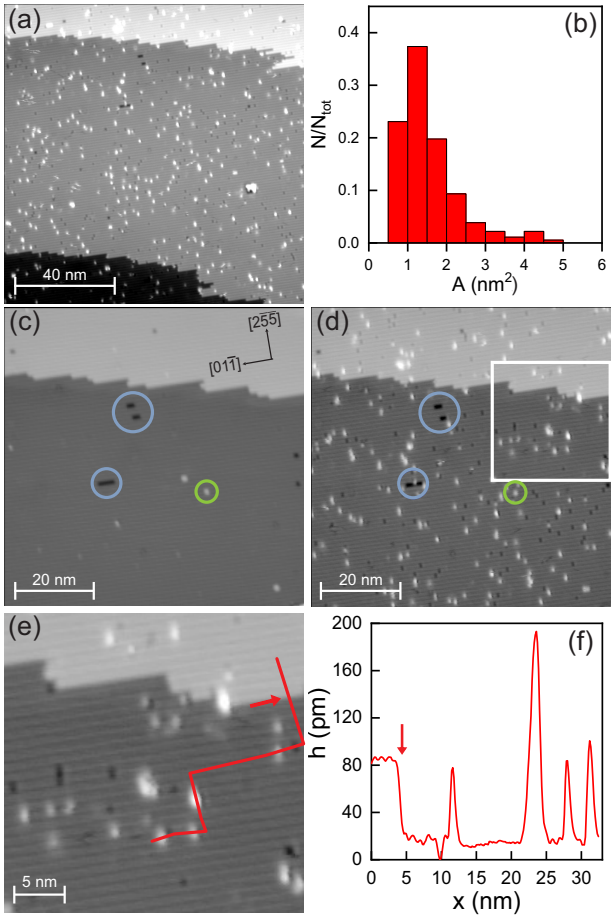


Fig. 2 Laser-induced creation of adatom and vacancy clusters at a 4 s irradiation at 9 mJ/cm$^2$ absorbed average fluence: (a) Large scale image after irradiation, local coverage: 0.07 ML; absorbed local fluence of $(0.5 \pm 0.05)$ mJ/cm$^2$ (b) Cluster area distribution from (a) normalized to the total number of clusters $N_{tot} = 221$ (c,d) STM images before (c) and after (d) laser irradiation, the same defects are encircled in (c) and (d) for reference (e) high-resolution image of square marked in (d); (f) height profile along line marked in (e); arrows in (e) and (f) mark the position of the secondary step edge; the images were recorded at -200 mV and (a,d,e) 20 pA and (c) 50 pA.

later laser pulses. The differing quantities of clusters result from variations in the laser-induced diffusion yield for the two types of particles.

To form clusters on the surface, vacancy-interstitial pairs must first be created in the bulk, and then these two species need to be transported to the surface. These processes can be induced either through direct interaction with energetic electrons or through heat transfer after the electrons have thermalized with the phonon system. We estimate that at the fluence used, the maximum phonon temperature reaches only 105 K, while an electron temperature of 3530 K is achieved based on the two-temperature model[37]. The phonon temperature is far below a temperature at which the described processes would occur thermally. The changes, thus, originate from the hot electrons, consequently demanding ultrashort laser irradiation. This notion is confirmed by a non-linear fluence dependence below.

We anticipate that the adatom and vacancy clusters will remain stable on the Cu(511) surface up to approximately 180 K. This expectation is based on earlier findings from studies on the Cu(100) surface, which is the face of the Cu(511) terraces[38–40]. Both adatoms and vacancies should exhibit mobility that allows for their annihilation, with adatoms needing to descend into vacancies.

On the Cu(100) surface, adatoms have a higher activation energy of 0.52 eV than vacancies[39]. Adatom diffusion becomes activated on experimental time scales at around 140 K[38]. Additionally, overcoming the Ehrlich-Schwoebel barrier, which restricts downward mass transport, requires an extra 0.125 eV[40]. The threshold temperature is estimated from these values, assuming that the prefactors for terrace and downward diffusion are identical.

### 3.3 Position-dependent alteration of the surface texture

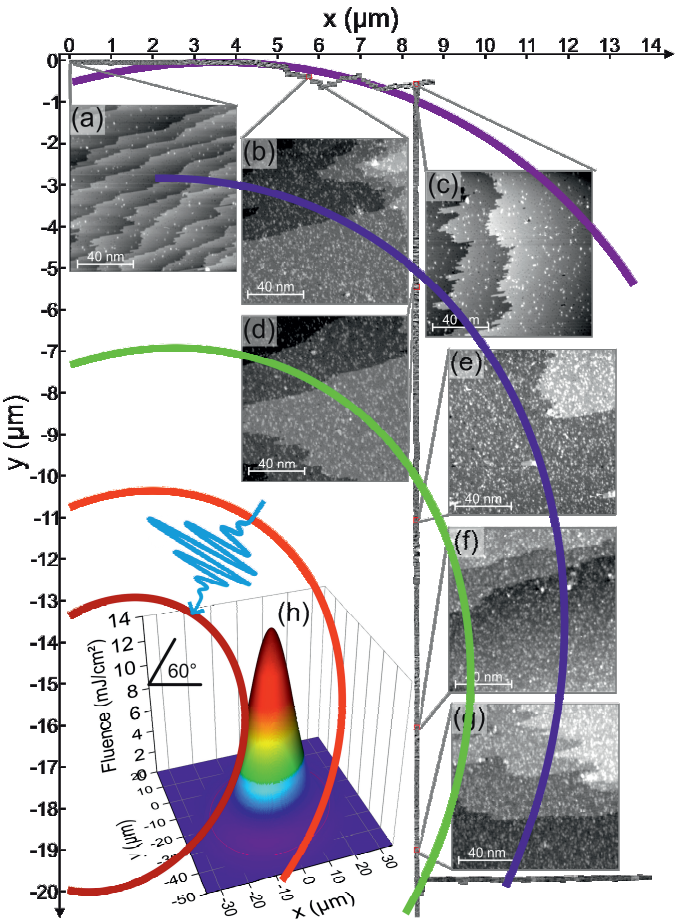


Fig. 3 Spatial surface modifications across the laser spot: Adjacent images recorded after a 1 s irradiation at 7.8 mJ/cm$^2$ absorbed fluence: (a to g) marked STM images enlarged; the images were recorded at -200 mV and between 6 pA and 20 pA (h) Spatial distribution of absorbed power of the laser spot calculated from the measured photoelectron signal at a laser power of 13.15 mW at the sample, corresponding to an absorbed power of 9.18 mW; ellipses in the main image reflect the colors of the distribution.

The images presented thus far depict the situation at a specific

View Article Online
DOI: 10.1039/D5NH00836K



point on the surface and correspond to a particular locally absorbed fluence within the laser spot. While this fluence remains relatively constant at the scale of an STM image, it varies significantly depending on the position of the STM image within the Gaussian profile of the laser spot, which spans several 10 $\mu$m (Fig. 3h). To investigate the fluence dependence of the observed defect creation, we captured 106 adjacent images in the x-direction, 223 images in the y-direction, and an additional 71 images in the x-direction. This approach covers distances of 8.8 $\mu$m, 19.9 $\mu$m, and 6.2 $\mu$m, respectively (Fig. 3). The complete set of images is provided in the Supplementary Information.

We discuss changes qualitatively at the first series. The series begins at (0,0) close to the tip position during irradiation. Very little material is generated on the surface at (0,0) at a locally absorbed fluence of 0.51 mJ/cm$^2$. (Fig. 3a). More material is created at all other explored regions, up to 25 $\mu$m from (0,0). It corroborates that the additional material does not result from the tip, as inferred earlier[27,28].

The coverage increases in the $x$-direction, reaching a maximum between x = 5 $\mu$m and x = 6 $\mu$m (Fig. 3b), and then decreases to a lower level at x = 8.5 $\mu$m, almost as low as at (0,0) (Fig. 3c). It demonstrates that the variations in locally absorbed fluence influence the amount of material driven to the surface.

For a quantitative analysis, we cover a larger spatial range in a region of the laser spot. When examining the coverage in the y-direction, a similar level of coverage to that in Fig. 3b is observed at approx. y = 5.5 $\mu$m (Fig. 3d). The coverage continues to increase (Fig. 3e) up to approximately y = 16 $\mu$m (Fig. 3f). Beyond this maximum, the coverage decreases (Fig. 3g).

### 3.4 Fluence-dependent alteration of the surface texture

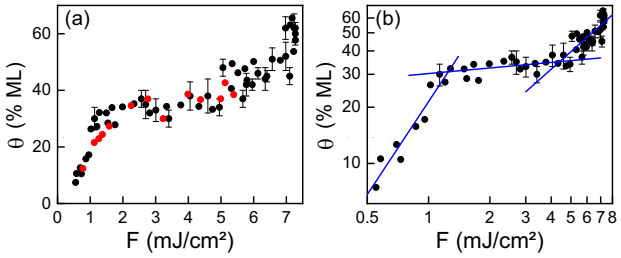


Fig. 4 Fluence-dependent coverage: (a,b) Coverage $\theta$ vs. locally absorbed fluence $F$ on linear (a) and double-logarithmic scale (b); black symbols: data from y-axis; red symbols: data from second x-axis; apparent linear fits in panel (b) yield slopes of $1.65 \pm 0.16$ up to 1.3 mJ/cm$^2$, $0.10 \pm 0.04$ between 1.3 mJ/cm$^2$ and 5 mJ/cm$^2$, and $0.97 \pm 0.19$ above 5 mJ/cm$^2$.

In the examined fluence range, the amount of material varies, yet the formed surface structures remain qualitatively similar. Therefore, a valuable descriptor for the change in surface texture is the amount of material produced. For a quantitative analysis, we specifically focus on regions of the surface that have larger terraces to minimize uncertainty caused by the presence of step edges. Notably, the coverage does not only depend on locally absorbed fluence, but the dependence varies across different fluence ranges, particularly changing at approximately 1.5 mJ/cm$^2$ and 5 mJ/cm$^2$ (Fig. 4a).

The relationship between fluence and coverage is linear on a double logarithmic scale (Fig. 4b). It indicates a power-law relationship, reflecting (multi-)photon laser-induced processes, commonly referred to as DI(M)ET (dynamics induced by (multiple) electronic transitions)[31]. In the context of femtosecond laser-induced processes at surfaces, an apparent slope of 1 suggests a linear dependence on fluence, a single-photon process, while a slope greater than 1 indicates a multi-photon process[31]. Up to a fluence of 1.3 mJ/cm$^2$, the slope is, at approximately 1.65, greater than one, suggesting a nonlinear process. Above 1.3 mJ/cm$^2$ and up to 5 mJ/cm$^2$, the slope decreases by a factor of 16, resulting in an unusual weak dependence on fluence. Consequently, the amount of material produced shows minimal change. This slight variation in the intermediate fluence range implies an (almost) fluence-independent surface texture. Above 5 mJ/cm$^2$, the slope increases again, but the linear slope should be interpreted cautiously due to the uncertainty for determining the larger coverages of a roughened surface. At higher fluences, the surface becomes increasingly rough due to an increasing number of adatom clusters of similar size, but reliable quantitative analysis is no longer feasible.

We further confirm the fluence-independent range by analyzing the second x series, where the data points align with those from the y series (Fig. 4a, red data points). We relate the differing slopes to the differing bulk diffusion rates of the created interstitials and bulk vacancies. At low fluence levels, only the vacancies created at the surface affect the coverage, while interstitials are also driven from the bulk to the surface. The slope of 1.65 suggests that one of the two processes contributing in this fluence range, vacancy-interstitial creation or interstitial diffusion, is a two-photon process. It is likely that the higher energy process, the creation of vacancy-interstitial pairs, is non-linear rather than the diffusion of the interstitials[41].

Beyond a fluence of 1.5 mJ/cm$^2$, bulk vacancies are also driven by the laser to the surface. These vacancies largely compensate for the additional created adatoms, resulting in a nearly constant coverage.

After the equilibration of adatoms and vacancies – when the same number reaches the surface – the non-linear nature of the processes once again leads to an increased coverage with higher fluence. Overall, our data demonstrate a pronounced non-monotonic surface modification that results from bulk-created defects influenced by locally absorbed fluence with a fluence-independent range between 1.3 mJ/cm$^2$ and 5 mJ/cm$^2$. We suggest to target this fluence range for a largely homogeneous effect of laser structuring across a laser spot.

We finally examine the surface structures formed in the three fluence ranges using selected images (Fig. 5). Generally, as the fluence increases, the range of cluster sizes also expands, while their overall number decreases (Fig. 5c,f,i).

The example with a locally absorbed fluence of 0.55 mJ/cm$^2$ falls within the non-linear fluence range. At this fluence, the additional material amounts to 0.07 ML. Clusters with areas smaller than 1.5 nm$^2$ and 2.0 nm$^2$ dominate, comprising 70% and 80%

View Article Online
DOI: 10.1039/D5NH00836K



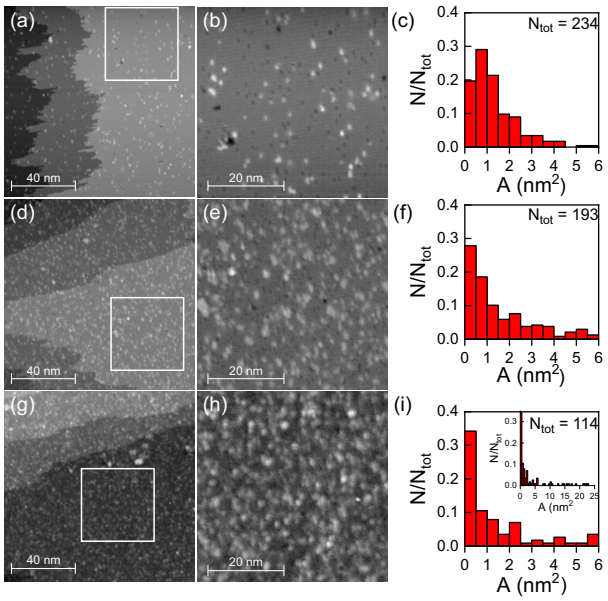


Fig. 5 Laser-induced creation of surface material in different locally absorbed fluence ranges: (a-c) Locally absorbed fluence of 0.55 mJ/cm$^2$ at x = 0.31 $\mu$m (d-f) Locally absorbed fluence of 2.32 mJ/cm$^2$ at x = 3.54 $\mu$m (g-i) Locally absorbed fluence of 7.11 mJ/cm$^2$ at x = 4.9 $\mu$m (a,d,g) Large-scale STM images, 20 pA, -200 mV (b,e,h) Small-scale STM images of the regions marked in (a,d,g), 20 pA, -200 mV (c,f,i) Area histograms, $N_{tot}$ is the total number of clusters.

of the adatoms, respectively (Fig. 5c). These clusters consist of only a few atoms. A locally absorbed fluence of 2.32 mJ/cm$^2$ represents the fluence-independent range. Here, the coverage is approximately 0.35 ML. Despite this significant increase in coverage, there remains a preference for smaller clusters, with 57% (and 62%) of the clusters still below the specified area thresholds (Fig. 5f). The slight increase in larger adatom clusters indicates that the smaller clusters formed during laser irradiation only merge into larger clusters through accidental coalescence of nearby clusters rather than through cluster diffusion.

The locally absorbed fluence of 7.11 mJ/cm$^2$ represents the linear fluence range. At a coverage of 0.66 ML, the sizes of the adatom clusters vary considerably; nevertheless, about half of them (52% to 56%) are classified as small (Fig. 5i). Only a few clusters contain several hundred atoms and occupy an area greater than 25 nm$^2$ (Fig. 5i, inset). The irregular shapes of the clusters at this high density (shown in Fig. 5h) confirm that they primarily form through accidental coalescence. Clusters generated from interstitials reaching the surface only coalesce when they are in close proximity to one another.

There is no significant qualitative difference in the structures created across different fluence ranges, unlike on the Cu(111) surface[28]. On the vicinal Cu(511) surface, laser-induced surface diffusion and cluster equilibration are suppressed. As a result, the surface texture relies entirely on bulk processes.

## Conclusions

A real-space investigation with nanometer precision over a micrometer-sized laser spot demonstrates that ultrashort laser pulses significantly alter the surface texture of a vicinal surface. The laser produces vacancy-interstitial pairs within the bulk material and propels them to the surface, even at energies below the threshold for laser ablation.

The most intriguing finding of this study is the identification of a fluence range between 1.3 mJ/cm$^2$ and 5 mJ/cm$^2$ in which the texture of the Cu(511) surface remains largely independent of fluence due to competing bulk processes. Within this fluence-independent range, the fluence increases almost fourfold. While the exact fluence range may vary depending on the material, we anticipate that the interaction of various laser-driven processes will produce similar results across different materials, giving a fluence range where the structural changes remain minimal. Our study also suggests that adjusting the size of a Gaussian-shaped laser spot can ensure that this fluence range encompasses the target material. On a broader scale, our research emphasizes the need for high-resolution local information to better understand the effects of ultra-short laser irradiation on materials and their properties.

Our study advances the understanding of light-induced pattern formation at the nanoscale[43]. Since processes occurring at or near surfaces are significantly affected by surface roughness, it is essential to consider these changes in surface texture across various fields, including femtochemistry, photocatalysis, atmospheric reactions, and even battery research[46]. The implications for femtochemistry and photocatalysis arise from the way turnover rates of surface reactions depend on surface structure[42]. Therefore, any femtochemical reaction that occurs at a comparable or higher fluence will benefit from the roughening of the surface. This indicates that the changed surface texture must be taken into account during interpretation. The same applies to experiments at higher temperatures than those used in this study, as surfaces can be temporarily altered during the timescale of a chemical reaction, even if the temperature exceeds the level at which defects are eliminated.

This surprising result will influence the understanding of all processes induced by ultra-short laser illumination, including, but not limited to, laser melting, ablation, and femtochemistry. To fully exploit fluence independence, we propose shaping the laser spot profile, for instance, by using hollow modes, i.e., doughnut-shaped profiles. In future, surface design will profit from the understanding of the microscopic mechanisms occurring under the highly non-equilibrium conditions formed in the near-surface region of a metal by ultra-short laser illumination.

## Author contributions

Niklas Osterloh: Investigation, Methodology, Validation, Formal analysis, Visualization, Writing - Review & Editing; Michael Vyshnepolsky: Investigation, Visualization, Methodology; Tianluo Pan: Investigation, Methodology; Karina Morgenstern: Conceptualization, Supervision, Resources, Data Curation, Writing – original draft; Writing - Review & Editing, Visualization, Project administration, Funding acquisition, Resources

## Conflicts of interest

There are no conflicts to declare.

View Article Online
DOI: 10.1039/D5NH00836K



## Data availability

Data is beyond that provided in the Supporting Information is available from the authors upon request.

## Acknowledgements

The authors express their gratitude to the German Science Foundation (DFG) for funding support through project MO 960/25-1 and the collaborative research centre CRC 1625, project no. 506711657.

## Notes and references

1 A. M. Lindenberg, J. Larsson, K. Sokolowski-Tinten, K. J. Gaffney, C. Blome, O. Synnergren, J. Sheppard, C. Caleman, A. G. MacPhee, D. Weinstein, D. P. Lowney, T. K. Allison, T. Matthews, R. W. Falcone, A. L. Cavalieri, D. M. Fritz, S. H. Lee, P. H. Bucksbaum, D. A. Reis, J. Rudati, P. H. Fuoss, C. C. Kao, D. P. Siddons, R. Pahl, J. Als-Nielsen, S. Duesterer, R. Ischebeck, H. Schlarb, H. Schulte-Schrepping, T. Tschentscher, J. Schneider, D. von der Linde, O. Hignette, F. Sette, H. N. Chapman, R. W. Lee, T. N. Hansen, S. Techert, J. S. Wark, M. Bergh, G. Huldt, D. van der Spoel, N. Timneanu, J. Hajdu, R. A. Akre, E. Bong, P. Krejcik, J. Arthur, S. Brennan, K. Luening, and J. B. Hastings, Atomic-Scale Visualization of Inertial Dynamics. *Science*, 2005, **308**, 392.

2 P. T. Mannion, J. Magee, E. Coyne, G. M. O'Connor, and T. J. Glynn, The Effect of Damage Accumulation Behaviour on Ablation Thresholds and Damage Morphology in Ultrafast Laser Micro-Machining of Common Metals in Air. *Appl. Surf. Sci.*, 2004, **233**, 275.

3 K. Sugioka and Y. Cheng, Ultrafast Lasers - Reliable Tools for Advanced Materials Processing. *Light: Sci. Appl.*, 2014, **3**, e149.

4 E. G. Gamaly and A. V. Rode, Physics of Ultrashort Laser Interaction with Matter: from Phonon Excitation to Ultimate Transformations. *Prog. Quant. Electron.*, 2013, **37**, 215.

5 R. R. Gatass and E. Mazur, Femtosecond Laser Micromachining in Transparent Materials. *Nature Phot.*, 2008, **2**, 219.

6 L. Jiang, A. Wang, B. Li, T. H. Cui, and Y.-F. Lu, Electrons Dynamics Control by Shaping Femtosecond Laser Pulses in Micro/Nanofabrication: Modeling, Method, Measurement and Application. *Light: Sci. Appl.*, 2018, **7**, 17134.

7 M. Z. Mo, Z. Chen, R. K. Li, M. Dunning, B. B. L. Witte, J. K. Baldwin, L. B. Fletcher, J. B. Kim, A. Ng, R. Redmer, A. H. Reid, P. Shekhar, X. Z. Shen, M. Shen, K. Sokolowski-Tinten, Y. Y. Tsui, Y. Q. Wang, Q. Zheng, X. J. Wang, and S. H. Glenzer, Heterogeneous to Homogeneous Melting Transition Visualized with Ultrafast Electron Diffraction. *Science*, 2018, **360**, 1451.

8 A. H. A. Lutey, L. Gemini, L. Romoli, G. Lazzini, F. Fuso, M. Faucon, and R. Kling, Towards Laser-Textured Antibacterial Surfaces. *Sci. Rep.*, 2018, **8**, 10112.

9 D. Hu, Y. Lu, Y. Cao, Y. Zhang, Y. Xu, W. Li, F. Gao, B. Cai, B.-O. Guan, C.-W. Qiu, and X. Li, Laser-Splashed Three-Dimensional Plasmonic Nanovolcanoes for Steganography in Angular Anisotropy. *ACS Nano*, 2018, **12**, 9233.

10 P. Fan, R. Pan, and M. Zhong, Ultrafast Laser Enabling Hierachical Structures for Versatile Superhydrophobicity with Enhanced Cassie-Baxter Stability and Durability. *Langmuir*, 2019, **35**, 16693.

11 C. Wang, H. Huo, M. Johnson, M. Shen, and E. Mazur, The Thresholds of Surface Nano-/Micro-Morphology Modifications with Femtosecond Laser Pulse Irradiations. *Nanotechnology*, 2010, **21**, 075304.

12 E. Allahyari, J. JJ Nivas, G. Avallone, M. Valadan, M. Singh, V. Granata, C. Cirillo, A. Vecchione, R. Bruzzese, C. Altucci, S. Amoruso, Femtosecond Laser Surface Irradiation of Silicon in Air: Pulse Repetition Rate Influence on Crater Features and Surface Texture. *Opt. Laser Technol.*, 2020, **126**, 106073.

13 R. Stoian and J. Bonse, *Ultrafast Laser Nanostructuring. Springer Series in Optical Sciences*, Vol 239. Springer, Cambridge, 2023.

14 Y. Miyasaka, M. Hashida, Y. Ikuta, K. Otani, S. Tokita, S. Sakabe, Nonthermal Emission of Energetic Ions from a Metal Surface Irradiated by Extremely Low-Fluence Femtosecond Laser Pulses. *Phys. Rev. B*, 2012, **86**, 075431.

15 H. Wang, Y.-L. Zhang, H. Xia, Q.-D. Chen, K.-S. Lee, and H.-B. Sun, Photodynamic Assembly of Nanoparticles towards Designable Patterning. *Nanoscale Horiz.*, 2016, **1**, 201.

16 Y. Zhang, L. Shi, D. Hu, S. Chen, S. Xie, Y. Lu, Y. Cao, Z. Zhu, L. Jin, B.-O. Guan, S. Roggec, and X. Li, Full-Visible Multifunctional Aluminium Metasurfaces by in situ Anisotropic Thermoplasmonic Laser Printing. *Nanoscale Horiz.*, 2019, **4**, 601.

17 Q. Xiao, B. Ma, X. Fei, D.-W. Liu, X.-P. Zhai, X.-Y. Li, M.-J. Xiao, Y. Peng, Q. Wang, and H.-L. Zhang, Unveiling the Dimension-Dependence of Femtosecond Nonlinear Optical Properties of Tellurium Nanostructures. *Nanoscale Horiz.*, 2021, **6**, 918.

18 J. Israelachvili, N. Maeda, K. J. Rosenberg, and M. Akbulut, Effects of Sub-Angstrom (Pico-Scale) Structure of Surfaces on Adhesion, Friction, and Bulk Mechanical Properties. *J. Mat. Res.*, 2005, **20**, 1952.

19 X. Zhang, and J. Jia, Frictional Behaviour of Micro/Nanotextured Surfaces Investigated by Atomic Force Microscope: a Review. *Surf. Rev. Lett.*, 2015, **22**, 1530001.

20 D. J. O'Connor, B. A. Sexton, and R. St. C. Smart, *Surface Analysis Methods in Materials Science*. Springer, 2nd Edition, Berlin, 2003.

21 J. Byskov-Nielsen, J. M. Savolainen, M. S. Christensen, and P. Balling, Ultrashort Pulse Laser Ablation of Metals: Threshold Fluence, Incubation Coefficient and Ablation Rates. *Appl. Phys. A*, 2010, **101**, 97.

22 K. C. Phillips, H. H. Gandhi, E. Mazur, and S. K. Sundaram, Ultrafast Laser Processing of Materials: a Review. *Adv. Opt. Phot.*, 2015, **7**, 648.

23 Y. Dai, M. He, H. Bian, B. Lu, X. Yan, and G. Ma, Femtosecond Laser Nanostructuring of Silver Film. *Appl. Phys. A*, 2012, **106**, 567.

24 D. S. Ivanov and L. V. Zhigilei, The Effect of Pressure Relaxation on the Mechanisms of Short Pulse Laser Melting. *Phys.*

View Article Online
DOI: 10.1039/D5NH00836K



*Rev. Lett.*, 2003, **91**, 105701.

25 C. Wu and L. V. Zhigilei, Microscopic Mechanisms of Laser Spallation and Ablation of Metal Targets from Large-Scale Molecular Dynamics Simulations. *Appl. Phys. A*, 2014, **114**, 11.

26 R. Li, O. A. Ashour, J. Chen, H. E. Elsayed-Ali, and P. M. Rentzepis, Femtosecond Laser Induced Structural Dynamics and Melting of Cu(111) Single Crystal. An Ultrafast Time-Resolved X-Ray Diffraction Study. *J. Appl. Phys.*, 2017, **121**, 055102.

27 C. Zaum, N. Osterloh, R. Darkins, D. M. Duffy, A. L. Shluger, and K. Morgenstern, Real-Space Observation of Surface Structuring Induced by Ultra-Fast-Laser Illumination far Below the Melting Threshold. *Sci. Rep.*, 2021, **11**, 13269.

28 N. Osterloh, T. Pan, and K. Morgenstern, The Unexpected Impact of Low-Intensity Ultra-Short Laser Light on the Structure of Surfaces - Imaged in Real Space. *Nanoscale Horiz.*, 2023, **8**, 55.

29 M. Mehlhorn, H. Gawronski, L. Nedelmann, A. Grujic, and K. Morgenstern, An Instrument to Investigate Femtochemistry on Metal Surfaces in Real-Space. *Rev. Sci. Instr.*, 2007, **78**, 033905.

30 M. Mehlhorn, J. Carrasco, A. Michaelides, and K. Morgenstern, Local Investigation of Femtosecond Laser Induced Dynamics of Water Nanoclusters on Cu(111). *Phys. Rev. Lett.*, 2009, **103**, 026101.

31 C. Frischkorn and M. Wolf, Femtochemistry at Metal Surfaces: Nonadiabatic Reaction Dynamics. *Chem. Rev.*, 2006, **106**, 4207-4233.

32 M. Hu, J. JJ Nivas, M. Valadan, R. Fittipaldi, A. Vecchione, R. Bruzzese, C. Altucci, S. Amoruso, Ultrafast Laser Surface Irradiation of Silicon: Effects of Repetition Rate in Vacuum and Air. *Appl. Surf. Sci.*, 2022, **606**, 154869.

33 T. Michely and J. Krug, *Islands, Mounds, and Atoms*. Springer, New York, 2004.

34 K. Morgenstern, G. Rosenfeld, G. Comsa, M. R. Sœrensen, B. Hammer, E. Lægsgaard, and F. Besenbacher, Kinetics of Fast Island Decay on Ag(111). *Phys. Rev. B*, 2001, **63**, 045412.

35 C. Sprodowski and K. Morgenstern, Temperature-Dependent Change of the Fractal Dimension of Cu Dendrites on Cu(111). *New J. Phys.*, 2020, **22**, 063055.

36 J. Canet-Ferrer, E. Coronado, A. Forment-Aliaga, E. Pinilla-Cienfuegos, Correction of the Tip Convolution Effects in the Imaging of Nanostructures Studied Through Scanning Force Microscopy. *Nanotechnology*, 2014, **25**, 395703.

37 S. I. Anisimov, B. L. Kapeliovich, and T. L. Perel'man, Electron Emission from Metal Surfaces Exposed to Ultrashort Laser Pulses. *Sov. Phys. JETP*, 1974, **39**, 375.

38 M. Breeman, D. O. Boerma, Migration of Cu Adatoms on a Cu(100) Surface, Studied with Low-Energy Ion Scattering (LEIS). *Surf. Sci.*, 1992, **269/270**, 224-228.

39 G. Boisvert, L. J. Lewis, Self-Diffusion of Adatoms, Dimers, and Vacancies on Cu(100). *Phys. Rev. B*, 1997, **56**, 7543-7655.

40 R. Gerlach, T. Maroutian, L. Douillard, D. Martinotti, H.-J. Ernst, A Novel Method to Determine the Ehrlich-Schwoebel Barrier. *Surf. Sci.*, 2001, **480** 97-102.

41 S. M. Foiles, M. I. Baskes, M. S. Daw, Embedded-Atom-Method Functions for the fcc Metals Cu, Ag, Au, Ni, Pd, Pt, and their Alloys. *Phys. Rev. B*, 1986, **33**, 7983-7991.

42 F. Tao, M. Salmeron, Surface Restructuring and Predictive Design of Heterogeneous Catalysts. *Science*, 2024, **386**, 6724.

43 A. Rudenko and J. P. Colombier, How Light Drives Material Periodic Patterns Down to the Nanoscale. In: R. Stoian and J. Bonse (eds.), *Ultrafast Laser Nanostructuring*. Springer Series in Optical Sciences, Vol. 239. Springer, Chambridge, 2023.

44 X. Cui, Q. Ruan, X. Zhuo, X. Xia, J. Hu, R. Fu, Y. Li, J. Wang, and H. Xu, Photothermal Nanomaterials: A Powerful Light-to-Heat Converter. *Chem. Rev.*, 2023, **123**, 11, 6891.

45 N. Schröder, F. Nyenhuis, R. Baumann, L. Mulko, T. Kiedrowski, J. A. L'Huillier, and A. F. Lasagni, Heating Influence on Hierarchical Structures Fabricated by Direct Laser Interference Patterning. *Sci. Rep.*, 2022, **12**, 17728.

46 W. Pfleging, A. Meyer, U. Rist, P. Smyrek, Y. Sterzl, Y. Zheng, and P. Zhu, Laser Structuring and Functionalization of Nanoscaled Battery Materials, *Proc. SPIE* 12410, Nanoscale and Quantum Materials: From Synthesis and Laser Processing to Applications 2023, 1241002.

## Data Availability Statement

View Article Online
DOI: 10.1039/D5NH00836K

The data presented in this manuscript is supplied in the Supporting Information. Other data sets and further supporting data are available upon request.